HHS Public Access

Author manuscript

Nat Med. Author manuscript; available in PMC 2015 April 15.

Published in final edited form as:

Nat Med. 2014 April ; 20(4): 368–376. doi:10.1038/nm.3487.

MicroRNA-126-5p promotes endothelial proliferation and limits atherosclerosis by suppressing Dlk1

Andreas Schober[1,2,3,9], **Maliheh Nazari-Jahantigh**[1,2,9], **Yuanyuan Wei**[1,2], **Kiril Bidzhekov**[1], **Felix Gremse**[4], **Jochen Grommes**[5], **Remco T A Megens**[1], **Kathrin Heyll**[1,2], **Heidi Noels**[2], **Michael Hristov**[1], **Shusheng Wang**[6], **Fabian Kiessling**[4], **Eric N Olson**[7], and **Christian Weber**[1,2,3,8]

[1]Institute for Cardiovascular Prevention, Ludwig-Maximilians-University Munich, Munich, Germany. [2]Institute for Molecular Cardiovascular Research, Rheinisch-Westfälische Technische Hochschule (RWTH) Aachen University, Aachen, Germany. [3]DZHK (German Centre for Cardiovascular Research), Partner Site Munich Heart Alliance, Munich, Germany. [4]Department for Experimental Molecular Imaging, RWTH Aachen University, Aachen, Germany. [5]European Vascular Center Aachen-Maastricht, RWTH Aachen University, Aachen, Germany, and Medical University Maastricht, Maastricht, The Netherlands. [6]Department of Cell and Molecular Biology, Tulane University, New Orleans, Louisiana, USA. [7]Department of Molecular Biology, University of Texas Southwestern Medical Center, Dallas, Texas, USA. [8]Cardiovascular Research Institute Maastricht, University Maastricht, Maastricht, The Netherlands.

Abstract

Atherosclerosis, a hyperlipidemia-induced chronic inflammatory process of the arterial wall, develops preferentially at sites where disturbed laminar flow compromises endothelial cell (EC) function. Here we show that endothelial miR-126-5p maintains a proliferative reserve in ECs through suppression of the Notch1 inhibitor delta-like 1 homolog (Dlk1) and thereby prevents atherosclerotic lesion formation. Endothelial recovery after denudation was impaired in *Mir126*$^{-/-}$ mice because lack of miR-126-5p, but not miR-126-3p, reduced EC proliferation by derepressing

Correspondence should be addressed to A.S. (aschober@med.lmu.de) or C.W. (chweber@med.lmu.de).

[9]These authors contributed equally to this work.

Accession codes. The microarray data have been deposited in the National Center for Biotechnology Information Gene Expression Omnibus database under accession number GSE34262.

Note: Any Supplementary Information and Source Data files are available in the online version of the paper.

AUTHOR CONTRIBUTIONS

A.S. and C.W. designed the study, analyzed data and wrote the paper. M.N.-J. performed mouse experiments and collected and processed the histological and qRT-PCR data. Y. W. collected data and performed luciferase assays and mimic treatments. K.B. performed and analyzed *in vitro* experiments. F.G. and F.K. collected data and performed the fluorescence molecular tomography and computed tomography analyses. J.G. was involved in the analysis of human atherosclerotic lesions. R.T.M. performed the multi-photon microscopy analysis. K.H. collected data and processed the *in situ* hybridization and immunostaining data. H.N. performed immunoblots and *in vitro* experiments. M.H. performed flow cytometry analysis and cell culture experiments under flow conditions. S.W. and E.N.O. were involved in study design and contributed to the mouse experiments. A.S. and M.N.-J. contributed equally to the study. All authors discussed the results and commented on the manuscript.

COMPETING FINANCIAL INTERESTS

The authors declare no competing financial interests.

Dlk1. At nonpredilection sites, high miR-126-5p levels in endothelial cells confer a proliferative reserve that compensates for the antiproliferative effects of hyperlipidemia, such that atherosclerosis was exacerbated in *Mir126*$^{-/-}$ mice. In contrast, downregulation of miR-126-5p by disturbed flow abrogated EC proliferation at predilection sites in response to hyperlipidemic stress through upregulation of Dlk1 expression. Administration of miR-126-5p rescued EC proliferation at predilection sites and limited atherosclerosis, introducing a potential therapeutic approach.

Adult ECs lining the inside of blood vessels require shear stress generated by laminar flow to fully differentiate into a low-replicative endothelial phenotype[1–3]. Increased EC turnover occurs at sites of disturbed flow, such as arterial branches, presumably in response to apoptosis[4–9]. Damaged ECs can be replaced rapidly by proliferation of resident ECs, thus preventing frank denudation of the luminal sur-face[10,11]. Although ECs are highly adaptive to environmental cues, chronic activation during, for example, hyperlipidemia produces a dysfunctional arterial endothelium characterized by proadhesive properties, which drive the recruitment of monocytes[12,13]. Moreover, various cardiovascular risk factors, such as hyperlipidemia, diabetes and vascular inflammation, can induce EC injury and apoptosis during atherosclerosis[14,15]. However, the functional role and mechanisms involved in replicative endothelial regeneration during atherosclerotic lesion formation are currently incompletely understood.

Endothelial microRNAs (miRNAs) have crucial roles during vascular development and in the response to hemodynamic stress and inflammation[16]. The precursor miRNA pre-miR-126 gives rise to two mature strands, miR-126-3p and miR-126-5p, which are among the most abundant miRNAs in ECs[17,18]. Deletion of the gene encoding pre-miR-126 affects vascular integrity and angiogenesis during development without causing overt abnormalities after birth[17,19,20]. However, ischemic neovascularization is severely impaired in *Mir126*$^{-/-}$ mice[19], and transfer of miR-126-3p by microparticles released from apoptotic ECs limits atherosclerosis[21], indicating an essential role for miR-126 in the endothelial stress response.

Here we determined the role of the two miR-126 strands in endo-thelial repair. Our results indicate that miR-126-5p promotes the replicative regeneration of arterial ECs and thus prevents atherosclerotic lesion formation by regulating EC turnover.

RESULTS

Mir126 deletion impairs EC regeneration in injured arteries

To determine its contribution to endothelial repair, we crossed mice with a deletion of the gene encoding pre-miR-126 (ref. 19) with *Apoe*$^{-/-}$ mice, which develop hyperlipidemia and atherosclerotic lesions, and subjected both *Mir126*$^{-/-}$ *Apoe*$^{-/-}$ and *Mir126*$^{+/+}$ *Apoe*$^{-/-}$ control mice to endothelial denudation of the carotid artery. Compared to *Mir126*$^{+/+}$ *Apoe*$^{-/-}$ control mice, the lesion area in *Mir126*$^{-/-}$ *Apoe*$^{-/-}$ mice was significantly increased at days 14 and 28 after denudation (Fig. 1a). Whereas the lesional smooth muscle cell (SMC) area (Fig. 1b and Supplementary Fig. 1a) and collagen content (Fig. 1c) were unaffected by deletion of the *Mir126* gene, the lesional macrophage area was larger in *Mir126*$^{-/-}$ *Apoe*$^{-/-}$ mice than in control mice at days 14 and 28 (Fig. 1d) because of an increase in average cell

size but not in $Mac2^+$ cell number (Fig. 1e). Endothelial recovery of the luminal lining after complete removal of the endothelium (Supplementary Fig. 1b) was significantly impaired in *Mir126*$^{-/-}$ *Apoe*$^{-/-}$ compared to control mice at days 14 and 28 d (Fig. 1f), and this effect was accompanied by a reduced rate of EC proliferation at day 28 (Fig. 1g,h). Lesional $Mac2^+$ macrophages did not express the endothelial marker CD31 or the cell cycle–associated Ki67 antigen (Supplementary Fig. 1c).

Given that bone marrow (BM)-derived cells also express *Mir126* (ref. 22), we generated *Mir126*$^{-/-}$ *Apoe*$^{-/-}$ BM chimeras in a crossover study designed to dissect the roles of endothelial-resident and BM-derived miR-126. BM-derived miR-126 was unable to rescue endothe-lial repair during lesion formation in *Mir126*$^{-/-}$ *Apoe*$^{-/-}$ recipient mice (Fig. 1i,j). Taken together, these results indicate that *Mir126* deficiency impairs endothelial recovery by reducing cell proliferation, thereby promoting lesion formation.

Role of the miR-126-5p target Dlk1 in vascular repair

To identify direct targets of the two miR-126 strands that could potentially contribute to exacerbated lesion formation in *Mir126*$^{-/-}$ mice, we used microarrays to evaluate global gene expression in *Mir126*$^{-/-}$ *Apoe*$^{-/-}$ and *Mir126*$^{+/+}$ *Apoe*$^{-/-}$ mice 14 d after endothelial denudation. Compared with their expression levels in control mice, 513 genes were upregulated in the injured carotid arteries of *Mir126*$^{-/-}$ *Apoe*$^{-/-}$ mice (fold change ≥2.0, $P \leq 0.05$, $n = 4$ per group; Supplementary Table 1). Notably, the expression of known miR-126-3p targets, such as Spred1 or Vcam1, was not increased in *Mir126*$^{-/-}$ *Apoe*$^{-/-}$ mice (Supplementary Table 1). Among the upregulated genes, the mRNA encoding phosphodiesterase 6H (Pde6h) is a predicted target of miR-126-3p, and the mRNAs encoding Dlk1 and coiled-coil domain–containing protein 18 (Ccdc18) are predicted targets of miR-126-5p. However, only the upregulation of *Dlk1*, a noncanonical inhibitor of NOTCH1 (ref. 23), could be verified by quantitative RT-PCR (qRT-PCR) (Fig. 2a). We detected expression of Dlk1 protein in the injured artery, primarily in the CD31-positive endothelium covering the lesion (Fig. 2b) but not in SMCs or macrophages (Supplementary Fig. 2a), suggesting a functional involvement of this protein in endothelial recovery. To confirm that *Dlk1* is a direct target of miR-126-5p, we transfected HEK293 cells with a luciferase reporter vector containing the wild-type or mutated 3′ untranslated region (UTR) of *Dlk1* (Supplementary Fig. 2b). Co-transfection of the cells with synthetic miR-126-5p significantly reduced luciferase activity in cells expressing the wild-type *Dlk1* vector but had no effect on luciferase activity in cells expressing the mutant vector (Fig. 2c). Furthermore, miR-126-3p had no effect on the activity of the wild-type or mutant *Dlk1* 3′ UTR constructs (Supplementary Fig. 2c).

We next confirmed targeting of *DLK1* by miR-126-5p and studied the effects of DLK1 on proliferation of human umbilical vein ECs (HUVECs). Inhibition of miR-126-5p resulted in increased DLK1 expression and reduced EC proliferation, whereas overexpression of miR-126-5p had the opposite effect (Fig. 2d,e). The effects of inhibition and overexpression of miR-126-5p on EC proliferation were rescued by silencing or overexpression of *DLK1*, respectively (Fig. 2e). Similarly, treatment of the cells with a NOTCH1 inhibitor, SAHM1, reduced miR-126-5p–induced EC proliferation (Fig. 2e). In HUVECs overexpressing *DLK1*,

mutation of the miR- 126-5p binding site in its 3′ UTR attenuated the proliferative effect of a miR- 126-5p mimic (Fig. 2f).

In line with increased arterial expression of Dlk1 in *Mir126*$^{-/-}$ *Apoe*$^{-/-}$ mice, activation of Notch1 in the luminal ECs of injured arteries was significantly lower in *Mir*126$^{-/-}$ *Apoe*$^{-/-}$ mice as compared to *Mir126*$^{+/+}$ *Apoe*$^{-/-}$ mice (Fig. 2g). To study the role *of Dlk1* in endothelial repair, we used siRNA to silence *Dlk1* expression in *Mir126*$^{-/-}$ *Apoe*$^{-/-}$ mice 14 d after denudation. The *Dlk1*-specific siRNA reduced arterial *Dlk1* mRNA and protein expression (Fig. 2h), inhibited lesion formation (Fig. 2i) and enhanced endothelial recovery and EC proliferation (Fig. 2j). Similarly, EC-specific deletion of *Dlk1* in *Mir126*$^{+/+}$ *Apoe*$^{-/-}$ mice reduced lesion formation and increased endothelial proliferation 14 d after injury (Supplementary Fig. 2d,e). Taken together, these results indicate that the reduced EC proliferation in *Mir126*$^{-/-}$ mice is attributable to derepression of *Dlk1*.

The passenger strand miR-126-5p promotes endothelial repair

The passenger strands of miRNAs are typically degraded and therefore less abundant than the guide strands; however, we detected appreciable expression levels of both the miR-126-5p passenger strand and the miR-126-3p guide strand in various mouse tissues (Supplementary Fig. 3a). Furthermore, both miR-126-3p and miR-126-5p were localized to ECs in normal arteries (Supplementary Fig. 3b), and miR-126-5p was expressed in the ECs of injured arteries (Supplementary Fig. 3c). To delineate the differential roles of the two miR-126 strands in endothelial repair, we subjected denuded arteries of *Apoe*$^{-/-}$ mice to perivascular treatment with strand-specific miRNA inhibitors (antagomirs). qRT-PCR analyses confirmed the specific inhibitory effects of the two antagomirs on miR-126-3p and miR-126-5p expression (Fig. 3a). Notably, compared with a control antagomir, the miR-126-5p antagomir, but not the miR-126-3p antagomir, increased the lesion area (Fig. 3b) and the Mac2^{+} macrophage area (Fig. 3c) and impaired endothelial recovery (Fig. 3d) and EC proliferation in the luminal lining (Fig. 3e). The reduced EC proliferation in miR-126-5p antagomir–treated arteries was associated with increased levels of *Cdkn1a* and *Cdkn2b* mRNAs but not *Cdkn1b* mRNA (Fig. 3f).

Moreover, arteries treated with the miR-126-5p antagomir had higher levels of *Dlk1* mRNA and endothelial Dlk1 immunostaining than control arteries (Fig. 3g). Inhibition of miR-126-5p but not miR-126-3p also decreased the expression level of the Notch1 target gene *Hes5* in injured arteries (Fig. 3h). Gain- and loss-of-function experiments in HUVECs confirmed that miR-126-5p promotes *Hes5* expression (Supplementary Fig. 3d) and Notch1 activity (Supplementary Fig. 3e). However, treatment with the miR-126-5p antagomir did not increase the lesion area in injured carotid arteries of *Mir126*$^{-/-}$ *Apoe*$^{-/-}$ mice harboring *Mir126*$^{+/+}$ *Apoe*$^{-/-}$ BM cells (Supplementary Fig. 3f). Conversely, perivascular treatment with a miR-126-5p mimic reduced lesion formation (Fig. 3i) and promoted endothelial recovery and EC proliferation (Fig. 3j) in *Apoe*$^{-/-}$ mice. These results indicate that increased EC proliferation and reduced lesion formation in *Mir126*$^{-/-}$ mice are attributable to the absence of miR-126-5p expression.

Site-specific effect of *Mir126* deletion on atherosclerosis

Atherosclerosis develops preferentially at predilection sites of the arterial tree with disturbed laminar flow, such as arterial branching points and the lesser curvature of the aortic arch, whereas nonpredeliction sites with laminar flow are protected from lesion formation. To evaluate the role of miR-126–mediated endothelial regeneration in a model of atherosclerosis without denudation, we fed *Apoe*$^{-/-}$ mice a high-cholesterol diet (HCD) only. Lesion formation at nonpredilection sites of the thoracoabdominal aorta (Fig. 4a), but not at predilection sites or in the aortic root (Fig. 4a,b), was markedly exacerbated by knockout of *Mir126*. The expression levels of miR-126-5p and miR-126-3p were lower in the aortic root of *Apoe*$^{-/-}$ mice than elsewhere in the aorta (Fig. 4c); this region-specific suppression was associated with increased expression of *Dlk1* mRNA (Fig. 4c). Moreover, compared with nonpredilection sites, miR-126-5p expression was lower, *Dlk1* mRNA and protein expression were higher and miR-126-3p expression was unaltered at predilection sites of *Apoe*$^{-/-}$ aortas (Fig. 4d and Supplementary Fig. 4a).

The deletion of *Mir126* also resulted in increased lesion formation (Fig. 4e), reduced angiographic lumen diameter (Fig. 4f) and increased lesional Mac2^{+} macrophage area (Fig. 4g) and cathepsin activity (Fig. 4h) in carotid arteries. Moreover, endothelial Dlk1 abundance was significantly higher in the carotid arteries of *Mir126*$^{-/-}$*Apoe*$^{-/-}$ mice than in those of *Mir126*$^{+/+}$ *Apoe*$^{-/-}$ mice (Fig. 4i). In contrast to the aortic root (Supplementary Fig. 4b), miR-126 deficiency reduced luminal EC proliferation in the carotid artery (Fig. 4j and Supplementary Fig. 4c). Notably, aortic wall expression of the miR-126-3p target vascular cell adhesion molecule 1 (Vcam-1), which has an important role in the development of atherosclerosis[24,25], was not affected by genetic deletion of *Mir126* (Supplementary Fig. 4d). These results indicate that miR-126 deficiency increases atherosclerosis at nonpredilection sites only, where miR-126-5p levels are higher than at predilection sites.

Disturbed flow reduces miR-126-5p to promote atherogenesis

To assess whether disturbed blood flow can reduce miR-126-5p expression, we generated a region of low shear stress by partial liga-tion of the carotid artery in *Apoe*$^{-/-}$ mice[26]. A significant reduction in miR-126-5p levels was evident 3 d after partial ligation; this effect preceded increased expression of both *Dlk1* mRNA, which occurred after 1 week (Fig. 5a), and Dlk1 protein, which occurred after 6 weeks (Fig. 5b). Dlk1 protein expression was also increased in intact, non-ligated carotid arteries of *Mir126*$^{-/-}$ mice as compared to *Mir126*$^{+/+}$ mice (Fig. 5b). In contrast to the progressive decrease of miR-126-5p expression, miR-126-3p expression levels were comparable at 1 d and 1 week after partial ligation (Fig. 5a). Accordingly, shear stress of HUVECs induced KLF2-dependent expression of pri-miR-126, leading to a marked accumulation of miR-126-5p but not miR-126-3p (Supplementary Fig. 5a,b). This result suggests the existence of different degradation mechanisms for the two strands. The upregulation of miR-126-5p by shear stress suppressed *Dlk1* mRNA and protein expression (Supplementary Fig. 5c–e) and increased EC proliferation through targeting of the miR- 126-5p binding site in the *Dlk1* 3′ UTR (Supplementary Fig. 5f).

In line with the downregulation of miR-126-5p observed after partial ligation, knockout of *Mir126* had no effect on lesion formation (Fig. 5c) or luminal EC proliferation (Fig. 5d) in

partially ligated carotid arteries *of Apoe*$^{-/-}$ mice. To assess whether disturbed flow promotes lesion formation through downregulation of miR-126-5p, we systemically treated *Mir126*$^{-/-}$ *Apoe*$^{-/-}$ mice after partial ligation of the carotid artery with miR-126-5p mimics, which resulted in uptake of miR-126-5p by aortic ECs (Supplementary Fig. 6a). The miR-126-5p mimic reduced lesion formation caused by acutely disturbed flow (Fig. 5e). This effect was associated with increased EC proliferation (Fig. 5f) and Notch1 activity (Fig. 5g), but reduced Dlk1 abundance (Fig. 5h), in luminal ECs of partially ligated carotid arteries. Moreover, silencing of *Dlk1* reduced disturbed flow–induced lesion formation (Fig. 5i) and increased EC proliferation (Fig. 5j) in *Mir126*$^{+/+}$ *Apoe*$^{-/-}$ mice. These results indicate that disturbed flow suppresses miR-126-5p and promotes lesion formation through upregulation of Dlk1.

miR-126-5p mimics rescue EC proliferation in hyperlipidemia

To determine whether miR-126-5p has a role in atherogenesis, we systemically treated HCD-fed *Mir126*$^{-/-}$ *Apoe*$^{-/-}$ mice with a miR-126-5p mimic. Treatment with the miR-126-5p mimic reduced lesion formation in the aorta (Fig. 6a) and aortic root (Fig. 6b) and increased luminal EC proliferation (Fig. 6c and Supplementary Fig. 6b) and endothelial Notch1 activation (Supplementary Fig. 6c). The miR-126-5p mimic also reduced atherosclerosis and increased EC proliferation in the aortic root of *Mir126*$^{+/+}$ *Apoe*$^{-/-}$ mice fed the HCD for 28 d (Supplementary Fig. 7a,b). Moreover, the progression of atherosclerosis in the thoracoabdominal aorta (Fig. 6d) and aortic root (Fig. 6e) of *Mir126*$^{+/+}$ *Apoe*$^{-/-}$ mice was inhibited when we initiated the miR-126-5p mimic treatment 8 weeks into a 12-week HCD feeding program. Although EC proliferation was higher at predilection sites than nonpredilection sites in *Mir126*$^{+/+}$ *Apoe*$^{-/-}$ mice fed a normal diet, it was comparable at both sites in mice fed the HCD (Fig. 6f). Notably, treatment with miR-126-5p increased the EC proliferation rate at predilection sites but not nonpredilection sites (Fig. 6f). Similarly, endothelial-specific deletion of *Dlk1* in *Mir126*$^{+/+}$ *Apoe*$^{-/-}$ mice increased EC proliferation at predilection sites after feeding the HCD for 3 weeks (Supplementary Fig. 7c). Overall, these data support the concept that hyperlipidemia suppresses EC proliferation at predilection sites because downregulation of miR-126-5p expression induced by disturbed flow limits the regenerative reserve of ECs by derepressing *Dlk1*.

In human atherosclerotic lesions, levels of miR-126-5p, but not miR-126-3p (Supplementary Fig. 8a–**c**), were correlated with lower endothelial DLK1 abundance (Fig. 6g; $R^2 = 0.2288$, $P = 0.0181$), increased luminal EC proliferation (Fig. 6h and Supplementary Fig. 8d; $R^2 = 0.5477$, $P < 0.0001$) and reduced numbers of lesional CD68$^+$ macrophages (Fig. 6i; $R^2 = 0.1892$, $P = 0.0234$). These results suggest that higher miR-126-5p levels are also atheroprotective in humans and that treatment with miR-126-5p mimics may have therapeutic value in human atherosclerosis.

DISCUSSION

The results presented here show that miR-126-5p expression is essential for the replicative response of ECs to injury by targeting the negative regulator of EC proliferation, Dlk1. This mechanism preserves EC proliferation after hyperlipidemic stress and is responsible for

reduced lesion formation in regions of the arterial tree that are protected from atherosclerosis. By contrast, disturbed flow limits the proliferative reserve of ECs by suppression of miR-126-5p expression, and thus ECs at predilection sites fail to maintain their proliferation rate after hyperlipidemic injury. This inadequate EC proliferation promotes lesion formation, which can be rescued by administration of miR-126-5p.

Various metabolic and immune-mediated mechanisms induce EC injury and death, which may lead to EC detachment from the vascular wall and cause endothelial dysfunction[14]. Endothelial integrity is usually maintained through replacement of damaged ECs with proliferating, healthy ECs. Our findings indicate that high levels of miR-126-5p are essential for replicative endothelial regeneration in response to injury by suppressing Dlk1. Dlk1, encoded by a paternally expressed, imprinted gene, exists in a soluble and membrane-bound form and is widely expressed during development but is downregulated in most tissues after birth[27]. Also known as preadipocyte factor-1, DLK1 controls preadipocyte expansion by inhibiting G1- to S-phase progression during the cell cycle[28]. DLK1 also impairs angiogenesis by inhibiting EC proliferation, which has been attributed to its inhibitory effect on NOTCH1 activation[29]. In line with our results, reduced NOTCH1 activation can impair cell proliferation, presumably by suppression of its target gene *HES5* and upregulation of the cell cycle inhibitor CDKN1A[30]. Impaired endothelial repair can lead to increased permeability, which in turn can enhance the influx of low-density lipopro-tein (LDL) into the vessel wall, increase LDL uptake by macrophages and promote lesion formation[9,31].

Chronic EC injury by disturbed flow induces endoplasmic reticulum stress and apoptosis, which promotes lesion development at predilection sites of atherosclerosis[32,33]. The proliferation of apoptosis-resistant ECs is increased at predilection sites, and this proliferation may regenerate the injured endothelium[5]. Our results show that upregulation of Dlk1 at predilection sites, mediated by the suppression of miR-126-5p, negatively regulates EC proliferation. We propose that ECs at predilection sites adapt to the enhanced turnover that occurs in response to disturbed flow by downregulating miR-126-5p. Under hyperlipidemic conditions, however, EC proliferation at predilection sites is severely reduced, indicating that in regions of disturbed flow, the regulation of EC regeneration becomes maladaptive. Under these conditions, upregulation of Dlk1 impedes the regenerative response of ECs to the proapoptotic and antiproliferative effects of oxidized LDL[15,34]. Our findings show that administration of a miR-126-5p mimic to increase miR-126-5p levels rescues EC proliferation and limits lesion formation at predilection sites, demonstrating that insufficient EC proliferation promotes atherosclerosis. Conversely, elevated miR-126-5p levels in ECs at nonpredilection sites may balance the antiproliferative effects of laminar shear stress by suppressing Dlk1 and thus generate a proliferative reserve that maintains the EC proliferation rate in the presence of hyperlipidemic stress. Accordingly, we showed that lack of miR-126-5p expression promotes lesion formation mainly in nonpredilection sites, indicating that the increased regenerative capacity of ECs generated by high miR-126-5p levels limits the susceptibility to atherosclerosis in these regions.

Our findings also show that the sister strand of miR-126-5p, miR-126-3p, is not involved in endothelial repair after mechanical injury. Known targets of miR-126-3p such as Spred1

were not upregulated in injured arteries in *Mir126*$^{-/-}$ mice, a finding that may be attributable to targets of miR-126-3p that are induced during endothelial repair and compete for binding to miR-126-3p[35]. By contrast, similarly to the effects of endogenous miR-126-5p, delivery of exogenous miR-126-3p by endothelial microparticles promotes endothelial proliferation and repair[36]. The previous finding that endothelial-derived miR-126-3p can induce SMC replication after complete cessation of blood flow[37] was not evident in the models of atherosclerosis used here. In contrast to our finding that endogenous miR-126-3p does not affect lesion formation after arterial injury, delivery of miR-126-3p, released from apoptotic ECs, reduces atherosclerosis and enhances angiogenic cell recruitment[21]. Moreover, patients with increased risk of cardiovascular disease have reduced circulating levels of miR-126-3p[38,39]. Taken together with our results, these findings suggest dual functions of the miR-126 strands in atheroprotective endothelial regeneration. The protective effects of miR-126-3p derived from apoptotic ECs or circulating angiogenic cells may occur at predilection sites, where the replicative capacity of ECs is inadequate under conditions of hyperli-pidemic stress, complementing the role of miR-126-5p in regulating EC proliferation at nonpredilection sites (Fig. 6j)[21,40]. However, the atheroprotective effect of miR-126-3p may still require basal miR-126-5p expression, as lesion formation was not increased at predilection sites in *Mir126*$^{-/-}$ mice. Accordingly, systemic treatment with only miR-126-5p mimics ameliorated lesion formation, indicating that this approach may be useful for treating atherosclerosis.

METHODS

Methods and any associated references are available in the online version of the paper.

ONLINE METHODS

Mouse models

Mir126$^{-/-}$ mice[19] on a mixed genetic background were crossed with *Apoe*$^{-/-}$ mice (C57BL/6 background; The Jackson Laboratory, Bar Harbor, Maine). Male or female *Mir126*$^{-/-}$ *Apoe*$^{-/-}$ mice and *Mir126*$^{+/+}$ *Apoe*$^{-/-}$ litter-mates were subjected to wire injury or partial carotid ligation and were then fed a HCD comprising 21% crude fat, 0.15% cholesterol and 19.5% casein (Altromin GmbH, Lage, Germany) for 4 or 6 weeks[41,42]. Alternatively, female mice were fed the HCD for 12 weeks before being euthanized. *Dlk1*$^{flox/flox}$ mice were crossed with endothelial-specific Bmx-Cre^{ERT2} *Apoe*$^{-/-}$ mice to generate mice with a tamoxifen-inducible *Dlk1* knockout in ECs (EC-*Dlk1*$^{flox/flox}$)[43,44]. Male EC-*Dlk1*$^{flox/flox}$ mice were mated with female *EC-Dlk1*$^{+/+}$ mice to ensure that the floxed *Dlk1* allele was derived from the male mouse, as *Dlk1* is a maternally imprinted gene. EC-*Dlk1*$^{flox/flox}$ and *EC-Dlk1*$^{+/+}$ mice were intraperitoneally injected with tamoxifen (2 mg per 20 g body weight; Sigma-Aldrich Chemie GmbH, Munich, Germany) dissolved in neutral oil (Migyol, Sasol Germany GmbH, Hamburg, Germany) for 5 consecutive days. Wire injury of the carotid artery was performed by advancing a 0.36-mm flexible angioplasty guidewire by 1 cm using transverse arteriotomy of the external carotid artery, and endothelial denudation of the common carotid artery was achieved by three rotational passes[42]. BM transplantation was performed as described[45]. After *in situ* perfusion fixation

(4% paraformaldehyde) or immersion fixation (PAXgene, Qiagen GmbH, Hilden, Germany), carotid arteries and aortic roots were embedded in paraffin. To obtain samples from predilection sites, branch points of the aorta were excised after perfusion with RNAlater (Life Technologies GmbH, Darmstadt, Germany). Straight parts of the thoracoabdominal aorta were harvested to study gene expression at nonpredilection sites. All animal experiments were reviewed and approved by the local authorities (State Agency for Nature, Environment and Consumer Protection of North Rhein-Westphalia) in accordance with German animal protection laws.

Human carotid lesion samples

Human atherosclerotic lesion specimens were obtained during carotid endarterectomy One-half of each sample was immediately stored in RNAlater (Life Technologies), and the other half was fixed in paraformaldehyde. The Ethics Committee of the Medical Faculty at RWTH Aachen University approved the study protocol for the collection of human atherosclerotic plaque samples, and written informed consent was obtained from all participating subjects.

qRT-PCR

Total RNA was isolated using the mirVana miRNA isolation kit, the RecoverAll total nucleic acid isolation kit or TRIzol (all from Life Technologies). Expression levels of miRNAs were quantified using TaqMan miRNA (Life Technologies) or miScript (Qiagen) primer assays. Specific primer sets were designed, or TaqMan assays were used to determine mRNA expression levels. The PCRs were run on a 7900HT thermocycler (Life Technologies). Relative expression levels were normalized to either single or multiple reference genes (snoRNA-135, *Rnu1a*, RNU44 or U6 for miRNAs and *Gapdh*, *Actb* or 18s RNA for mRNA), scaled to the sample with the lowest expression and logarithmically transformed ($\log_2$ or $\log_{10}$). The levels of miR-126-3p and miR-126-5p in different mouse tissues detected using TaqMan assays were corrected for differences in PCR efficiency using qBase version 2.0 software (Biogazelle NV, Zwijnaarde, Belgium).

Immunostaining

Quantitative immunostaining was performed using primary antibodies for α-smooth muscle actin (1:200; 1A4; Dako Germany GmbH, Hamburg, Germany), Mac2 (1:400; M3/38; Cedarlane, Burlington, Canada), vWF (1:1,000; rabbit polyclonal; ab9378; Abcam, Cambridge, UK), CD31 (1:75; goat polyclonal; sc-1506; Santa Cruz Biotechnology, Inc., Dallas, USA), collagen type I (1:400; rabbit polyclonal; CL50151AP; Cedarlane), calponin (1:200; EP798Y; Abcam) and CD68 (1:100; PG-M1; Dako). Fluorescently labeled secondary antibodies were used for detection. The percentage of the area that was positively stained or the cell number (2–3 sections per mouse) was determined using ImageJ (1.43n) analysis software (NIH, USA). For double immunofluorescence staining, a rabbit monoclonal, (1:75; EPR3486(2); Abcam) or polyclonal (1:75; ABN40; EMD Millipore Corp., Billerica, USA) antibody for Dlk1, a rat monoclonal antibody for Ki67 (1:25; Tec-3; Dako) or a mouse monoclonal antibody for PCNA (1:75; PC10; Abcam) was used alongside endothelial-specific rabbit polyclonal antibodies for CD31 (Abcam) or an endothelial-

specific antibody for vWF (F8/86; Dako). Activated Notch1 in ECs was detected using a rabbit polyclonal antibody for cleaved Notch1 (1:10,000; ab9535; Abcam) followed by the antibody to vWF. Nonspecific primary antibodies were used as negative controls. Fluorescently labeled secondary antibodies (DyLight488 and 549; KPL, Inc., Gaithersburg, USA) were used for visualization. Digital images were acquired using a Leica DMLB or DM6000B fluorescent microscope (Leica Microsystems GmbH, Wetzlar, Germany).

Lesion quantification

Serial sections (5-μm thick) of the carotid arteries (3–5 sections per mouse) or the aortic roots (3–5 sections per mouse) were stained with Movat's pentachrome or elastic van Gieson stain. Only sections in which there was no sign of damage to the medium, such as rupture of the internal elastic lamina, were included in the analysis of the lesion area after wire injury of the carotid artery. The lesion area was quantified by planimetry using Diskus software (Hilgers, Bonn, Germany)[42]. Aortas were *en face* prepared and stained with Oil Red O and mounted onto slides, and then microscopic images were collected.

In situ detection of mature miR-126 strands

Paraffin-embedded sections (4- or 7-μm thick) of PAXgene-fixed (Qiagen) or paraformaldehyde-fixed arteries were hybridized with double digoxigenin (DIG)-labeled probes (50 nM miR-126-5p, 25 nM miR-126-3p, 50 nM or 25 nM scrambled or 5 nM U6) in hybridization buffer (all from Exiqon A/S, Vedbaek, Denmark) at 52 °C (miR-126-3p, U6 and scrambled) or 42 °C (miR-126-5p and scrambled) for 1 h. Alternatively, after pepsin digestion (Dako), cooking in citrate buffer and digestion with RNase-free DNase (Roche Diagnostics GmbH, Mannheim, Germany), *in situ* detection was performed using DIG-conjugated dUTPs (Roche Diagnostics) for labeled extension on ultramer templates (rTth DNA Polymerase and EZ Buffer Pack, Life Technologies)[46]. The following ultramer templates were used: miR-126-5p, 5'-GACCCCTTAATGCGTCTAAAGACCCCTTAATGCGTCTAAAGACCCC TTAATGCGTCTAAACGCGTACCAAAAGTAATAATG-3′; and miR-126-3p, 5'-GACCCCTTAATGCGTCTAAAGACCCCTTAATGCGTCTAAAG ACCCC TTAATGCGTCTAAACGCATTATTACTCACGGTACGA-3′. After blockade of nonspecific (TNB blocking buffer, PerkinElmer, Inc., Waltham, MA, USA) and biotin/avidin (Blocking Kit, Vector Laboratories, Inc., Burlingame, CA, USA) binding sites, the sections were incubated with a peroxidase-conjugated antibody to DIG (1:100, 11207733910, Roche Diagnostics). A tyramide-based amplification system (TSA Plus Biotin, PerkinElmer) and Dylight 549-conjugated streptavidin (KPL) were used to visualize the probes.

Global gene expression analysis

Two weeks after wire injury, carotid arteries were harvested after *in situ* perfusion with RNAlater. A one-color-based hybridization protocol was applied (IMGM Laboratories GmbH, Munich, Germany) to 8 × 60K SurePrint G3 Mouse GE Microarrays (Agilent Technologies Germany GmbH, Böblingen, Germany). Quantile normalization and analysis of the raw data were performed using GeneSpring GX11.5 software (Agilent Technologies).

Prediction of miR-126-5p target genes

Among the genes expressed at least twofold higher in the carotid arteries of *Mir126*$^{-/-}$ *Apoe*$^{-/-}$ mice (as determined by global gene expression analysis), potential targets of miR-126-5p and miR-126-3p were identified using the TargetScan (http://www.targetscan.org/) and MicroCosm Targets (http://www.ebi.ac.uk/enright-srv/microcosm/htdocs/targets/v5/) target prediction algorithms.

Luciferase reporter assay

The full length 3′ UTR of mouse *Dlk1* was cloned into the psiCHECK-2 luciferase reporter vector (Promega Corporation, Madison, WI, USA) at the XhoI and NotI sites. To generate mutations at the miR-126-5p target site, PCR was performed using the following primers: 5′-ATGCAT GATAATGAAATTAAATAATAAGA-3′ and 5′-TAATTTCATTATCATGCA TTAATAGGGAG-3′. HEK293 cells were cultured in complete DMEM (PAA Laboratories GmbH, Cölbe, Germany) in 96-well plates. Lipofectamine 2000 (Life Technologies) was used to co-transfect subconfluent cells with 100 ng of the *Dlk1* 3′ UTR luciferase reporter vector or empty psiCHECK2 and 15 nM or 30 nM of synthetic miR-126-5p or miR-126-3p duplex (pre-miRNAs) or scrambled pre-miRNA (Life Technologies). Forty-eight hours after transfection, firefly and *Renilla* luciferase activities were measured using the Dual-Glo Luciferase Assay System (Promega) and a microplate reader (Tecan Group Ltd., Männedorf Switzerland). The *Renilla* luciferase activity was normalized to the firefly luciferase activity.

Antagomir treatment

The following antisense RNA oligonucleotides containing 2′-OMe-modified nucleotides (m), a partial phosphorothioate backbone (*) and a cholesterol group (Chol) were synthesized: miR-126-5p, 5′-mC(*)mG(*)mCm GmUmAmCmCmAmAmAmAmGmUmAm AmUmA(*)mA(*)mU(*)mG(*)-Chol-3′; and miR-126-3p, 5′-mC(*)mG(*)mCmAmUmUmAmUmUmAmCmU mCmAmCmGmGmUmA(*)mC(*)mG(*)mA(*)-Chol-3′ (Dharmacon, Fisher Scientific, Germany GmbH, Schwerte, Germany). The following control antagomir contained a random sequence of nucleotides and was not complementary to any known miRNA: 5′-mA(*)mU(*)mGmAmCmUmAmUmCmGmCmUm AmUmUmCmGmC(*)mA(*)mU(*)mG(*)-Chol-3′ (Dharmacon). Antagomirs (160 μg) were dissolved in 35% pluronic gel (Sigma-Aldrich). Perivascular antagomir treatment of the carotid arteries started 1 week after wire-induced injury and was repeated weekly.

siRNA application

One week after carotid injury of *Mir126*$^{-/-}$ *Apoe*$^{-/-}$ mice or partial carotid ligation of *Mir126*$^{+/+}$ *Apoe*$^{-/-}$ mice, 4 nmol of Dlk1-specific siRNAs (UCUUUCUCAACAAGUGCGA; UUAUCAAGUAUCAAAUAUA; GCAUGAUAAUGAAUAAUAA; CCUGCGUGAUCAAUGGUUC; SMARTpool Accell siRNA, Dharmacon) or a nonspecific siRNA (Dharmacon) dissolved in pluronic gel (35%) and supplemented with transfection reagent (Dharmafect 4, Dharmacon) was applied perivascularly[45]. The injured carotid arteries were harvested 1 week after the siRNA

treatment. After partial carotid ligation, perivascular treatment with siRNA was performed once per week, and the arteries were harvested at week 6.

Computed tomography (CT)

The diameters of the left and right common carotid arteries were determined by angiography using dual energy micro-CT (TomoScope DUO, CT Imaging, Erlangen, Germany) after intravenous injection of a blood pool contrast agent[47].

Fluorescence molecular tomography

Fluorescence molecular tomography (FMT 2500, PerkinElmer) was performed 24 h after the injection of a fluorescent probe (ProSense 680, PerkinElmer) sensitive to cathepsins. Carotid arteries were segmented on the basis of the micro-CT data to compute the corresponding amount of fluorescent dye in the quantitative three-dimensional tomography data (Imalytics Research Workstation, Philips Research, Eindhoven, the Netherlands).

Detection of EC proliferation and endothelial denudation *in vivo*

To detect DNA synthesis in ECs using two-photon laser scanning microscopy and three-dimensional deconvolution microscopy, mice were injected with 300 μg of EdU (Click-iT EdU Alexa Fluor 594 Imaging Kit, Life Technologies) 96, 72, 48 and 24 h before harvesting the carotid arteries and aortic arches.

For two-photon laser scanning microscopy, carotid arteries were isolated and *ex vivo* perfused (80 mm Hg)[48]. An Alexa Fluor 488-conjugated antibody against CD31 (2.5 μg ml^{-1}; 390, BD Biosciences, Heidelberg, Germany) was applied intraluminally for 30 min, and the artery was flushed with HBSS (Life Technologies). Subsequently, the azide-containing fluorescence dye (Alexa Fluor 594) was applied to the *ex vivo*-perfused carotid artery for 1 h to label EdU. The mounted arteries were imaged using an Olympus FV1000MPE two-photon laser scanning microscope coupled to a 25×1.05 numerical aperture (NA) water-dipping objective (Olympus Germany GmbH, Hamburg, Germany) and a MaiTai DeepSee Ti:Sa pulsed laser (Newport Spectra-Physics GmbH, Darmstadt, Germany) tuned at 780 nm. Emitted fluorescent signals were detected by three photomultiplier tubes (PMTs) tuned to the following wavelengths: autofluores-cence of extracellular matrix (PMT1), 400–510 nm; CD31 and Alexa Fluor 488 (PMT2), 510–560 nm; EdU and Alexa Fluor 594 (PMT3), 560–660 nm. Single images (1,024 × 1,024 pixels) were recorded in the *xy* plane and subsequently collected at successive depths (z stack; the distance between the *xy* planes was 1 μm). A Kalman image acquisition protocol (3× line scan) was used to repress the contribution of noise to the raw dataset. Two-photon laser scanning microscopy data were processed using ImagePro Analyzer 3D software (version 7.0, Media Cybernetics, Inc., Rockville, MD, USA).

To study the proliferation of ECs at predilection and nonpredilection sites, the left carotid artery and the adjacent part of the aortic arch were *en face* prepared (Supplementary Fig. 9), and CD31 immunostaining was combined with EdU labeling. EC coverage after wire injury was assessed in the *en face* prepared left carotid artery immunostained for CD31. The stained sections were visualized using a DM6000B microscope (Leica Microsystems)

equipped with a fully motorized stage and a digital camera (Leica DFC365 FX, Leica Microsystems). To detect the fluorescent signals in *en face* prepared aortas, *z* stacks of two-dimensional images were recorded, and deconvolution was performed using a mathematical algorithm to remove out-of-focus information (AF6000 3D deconvolution software module, Leica Microsystems).

Treatment with miR- 126-5p mimics

Synthetic miR-126-5p or negative control miRNAs (4464058) (*mir*Vana miRNA mimics, Life Technologies) were packaged in a nanoparticle carrier system (MaxSuppressor *In vivo* RNA Lancer Kit, Bio Scientific Corporation, Austin, TX, USA). HCD-fed *Mir126*$^{-/-}$ *Apoe*$^{-/-}$ mice or *Mir126*$^{+/+}$ *Apoe*$^{-/-}$ mice were intravenously injected with miR-126-5p or negative control mimics (100 μg per injection) every 72 h for 4 weeks of the HCD feeding or for the last 4 weeks of a 12-week HCD feeding program. In *Mir126*$^{-/-}$ *Apoe*$^{-/-}$ mice, partial ligation of the carotid artery was performed. Local treatment of the carotid artery with miR-126-5p or negative control mimics was performed by weekly perivascular application of the mimics (5 nmol per application, beginning 1 week after wire injury) dissolved in pluronic gel (35%) supplemented with Dharmafect 4 transfection reagent. Arteries and aortic roots were fixed using PAXgene Tissue Fix (Qiagen).

Cell culture

Lipofectamine 2000 was used to transfect HUVECs (Lonza Group Ltd, Basel, Switzerland) for 24–48 h with the following nucleic acids: LNA-modified miR-126-5p inhibitors (CGCGTACCAAAAGTAATAATG), LNA-modified miR-126-3p inhibitors (GCATTATTACTCACGGTACG) or nontargeting control oligonucleotides (GTGTAACACGTCTATACGCCCA) (100 nM each; Exiqon), miR-126-5p mimics, miR-126-3p mimics or negative control mimics (30 nM each; Life Technologies), bacterial artificial chromosomes (BACs) (WI2-1873 A7, BACPAC Resources, Children's Hospital Oakland, Oakland, CA, USA) containing wild-type *Dlk1* or *Dlk1* with a deletion of the miR-126-5p target site (AATAATAATAA) in the 3′ UTR (Quick and Easy BAC Modification Kit, Gene Bridges GmbH, Heidelberg, Germany) or the pPGK-*Dlk1* expression vector[49]. In addition, HUVECs were treated with the NOTCH1 inhibitor SAHM1 (15 μM; EMD Millipore). HUVECs (passage 3–5, 10^5 cells per cm^2) were cultured in a perfusion chamber (μ-Slides, ibidi GmbH, Martinsried, Germany) under shear stress (10 dyne cm^{-2}) generated by perfusion with medium using the ibidi Pump System. *Klf2* was silenced using an siRNA (30 pmol; 4392420, Silencer siRNA, Life Technologies). Proliferation of HUVECs was assessed using flow cytometry. In these experiments, the cells were fixed in ice-cold 70% ethanol and stained with a mixture of 20 μg ml^{-1} propidium iodide, 10 μg ml^{-1} RNase A and 0.1% Triton X-100 (all from Sigma-Aldrich). Sample acquisition and determination of the numbers of cells in the S, G1 and G2/M phases of the cell cycle were performed using an Attune Acoustic Focusing Cytometer (Life Technologies). Percentages of cells in the G2/M phase of the cell cycle normalized to the control group were calculated.

Determination of NOTCH 1 activity

NOTCH 1 activity in HUVECs was determined using a NOTCH1 pathway-responsive luciferase reporter assay (NOTCH1/CSL Reporter Kit, BPS Bioscience, Inc., San Diego, CA, USA) according to the manufacturer's instructions.

Western blot analysis

HUVECs were lysed in buffer comprising 50 mM Tris-HCl (pH 8.0), 150 mM NaCl, 1% Triton X-100, 2 mM EDTA and protease inhibitors (Complete Protease Inhibitor Cocktail, Roche Diagnostics). Cell lysates were resolved on SDS-PAGE gels and then transferred to polyvinylidene difluoride membranes. Proteins were detected using rabbit polyclonal antibodies against DLK1 (1:1,000, EPR3486(2), Abcam) and β-actin (1:8,000, AC-15, Abcam). Protein bands were visualized using an enhanced chemiluminescence detection system (ECL Advance, GE Healthcare GmbH, Munich, Germany) and an LAS 3000 Imager (Fuji Photo Film Co., Ltd., Tokyo, Japan) and were quantified using Multigauge software (Fuji Photo Film). Intensities of the DLK1 bands were expressed as a percentage of those of the β-actin bands.

ELISA

Proteins were isolated from carotid artery sections using the Qproteome FFPE Tissue Kit (Qiagen). The aortas were homogenized in cell lysis buffer (Cell Signaling Technology, Inc., Danvers, MA, USA) using a TissueLyser LT homogenizer (Qiagen). The levels of Dlk1 in the carotid arteries were determined using a mouse Dlk1 ELISA Kit (Cusabio Biotech, Wuhan, China). Vcam1 protein levels were measured using a mouse Vcam1 ELISA kit (RayBiotech, Inc., Norcross, GA, USA). Dlk1 and Vcam1 protein levels were normalized to the total protein concentration, which was quantified by DC Protein Assay Kit (Bio-Rad Laboratories GmbH, Munich, Germany). Absorbance at 450 nm was measured using an Infinite M200 plate reader (Tecan Group Ltd.)

Statistical analyses

To compare the experimental groups, Student's *t* test or one-way ANOVA followed by Newman-Keuls test was performed using Prism 5 software (GraphPad Software Inc., La Jolla, CA, USA). Data from the human plaque samples were analyzed using Pearson correlation calculations. $P < 0.05$ was considered to be statistically significant.

Supplementary Material

Refer to Web version on PubMed Central for supplementary material.

ACKNOWLEDGMENTS

A.S., F.K. and C.W. are funded by the Deutsche Forschungsgemeinschaft, Germany (FOR809, WE1913/11-2 and SCHO1056/3-2). A.S. and C.W. are funded by the German Federal Ministry of Education and Research (01KU1213A) and by the German Centre for Cardiovascular Research (MHA VD1.2). M.N.-J. was funded by the Interdisciplinary Centre for Clinical Research within the Faculty of Medicine at RWTH Aachen University, Germany. We thank J. Schmidt (University of Illinois) and R.H. Adams (Max-Planck-Institute for Molecular Biomedicine) for providing *Dlk1*^{flox} and Bmx-Cre^{ERT2} mice, respectively. We thank L. Natarelli, L. Pawig, J. Corbalán Campos, R. Soltan, M. Garbe, C. Geissler, P. Hartmann and S. Elbin for technical assistance.

References

1. Deanfield JE, Halcox JP, Rabelink TJ. Endothelial function and dysfunction: testing and clinical relevance. Circulation. 2007; 115:1285–1295. [PubMed: 17353456]
2. Aird WC. Phenotypic heterogeneity of the endothelium: I. Structure, function, and mechanisms. Circ. Res. 2007; 100:158–173. [PubMed: 17272818]
3. Ando J, Yamamoto K. Effects of shear stress and stretch on endothelial function. Antioxid. Redox Signal. 2011; 15:1389–1403. [PubMed: 20854012]
4. Chiu JJ, Chien S. Effects of disturbed flow on vascular endothelium: pathophysiological basis and clinical perspectives. Physiol. Rev. 2011; 91:327–387. [PubMed: 21248169]
5. Sakao S, et al. Initial apoptosis is followed by increased proliferation of apoptosis-resistant endothelial cells. FASEB J. 2005; 19:1178–1180. [PubMed: 15897232]
6. Kaiser D, Freyberg MA, Friedl P. Lack of hemodynamic forces triggers apoptosis in vascular endothelial cells. Biochem. Biophys. Res. Commun. 1997; 231:586–590. [PubMed: 9070851]
7. Schwartz SM, Benditt EP. Aortic endothelial cell replication. I. Effects of age and hypertension in the rat. Circ. Res. 1977; 41:248–255. [PubMed: 872300]
8. Wright HP. Endothelial mitosis around aortic branches in normal guinea pigs. Nature. 1968; 220:78–79. [PubMed: 5677450]
9. Foteinos G, Hu Y, Xiao Q, Metzler B, Xu Q. Rapid endothelial turnover in atherosclerosis-prone areas coincides with stem cell repair in apolipoprotein E- deficient mice. Circulation. 2008; 117:1856–1863. [PubMed: 18378610]
10. Hansson GK, Chao S, Schwartz SM, Reidy MA. Aortic endothelial cell death and replication in normal and lipopolysaccharide-treated rats. Am. J. Pathol. 1985; 121:123–127. [PubMed: 2996359]
11. Itoh Y, Toriumi H, Yamada S, Hoshino H, Suzuki N. Resident endothelial cells surrounding damaged arterial endothelium reendothelialize the lesion. Arterioscler. Thromb. Vasc. Biol. 2010; 30:1725–1732. [PubMed: 20558819]
12. Weber C, Noels H. Atherosclerosis: current pathogenesis and therapeutic options. Nat. Med. 2011; 17:1410–1422. [PubMed: 22064431]
13. Zhou Z, et al. Lipoprotein-derived lysophosphatidic acid promotes atherosclerosis by releasing CXCL1 from the endothelium. Cell Metab. 2011; 13:592–600. [PubMed: 21531341]
14. Pober JS, Min W, Bradley JR. Mechanisms of endothelial dysfunction, injury, and death. Annu. Rev. Pathol. 2009; 4:71–95. [PubMed: 18754744]
15. Chen CH, et al. Oxidized low-density lipoproteins inhibit endothelial cell proliferation by suppressing basic fibroblast growth factor expression. Circulation. 2000; 101:171–177. [PubMed: 10637205]
16. Neth P, Nazari-Jahantigh M, Schober A, Weber C. MicroRNAs in flow-dependent vascular remodelling. Cardiovasc. Res. 2013; 99:294–303. [PubMed: 23612583]
17. Fish JE, et al. miR-126 regulates angiogenic signaling and vascular integrity. Dev. Cell. 2008; 15:272–284. [PubMed: 18694566]
18. Wei Y, Nazari-Jahantigh M, Neth P, Weber C, Schober A. MicroRNA-126, −145, and −155: a therapeutic triad in atherosclerosis? Arterioscler. Thromb. Vasc. Biol. 2013; 33:449–454. [PubMed: 23324496]
19. Wang S, et al. The endothelial-specific microRNA miR-126 governs vascular integrity and angiogenesis. Dev. Cell. 2008; 15:261–271. [PubMed: 18694565]
20. Kuhnert F, et al. Attribution of vascular phenotypes of the murine Egfl7 locus to the microRNA miR-126. Development. 2008; 135:3989–3993. [PubMed: 18987025]
21. Zernecke A, et al. Delivery of microRNA-126 by apoptotic bodies induces CXCL12-dependent vascular protection. Sci. Signal. 2009; 2:ra81. [PubMed: 19996457]
22. Lechman ER, et al. Attenuation of miR-126 activity expands HSC in vivo without exhaustion. Cell Stem Cell. 2012; 11:799–811. [PubMed: 23142521]
23. Baladrón V, et al. dlk acts as a negative regulator of Notch1 activation through interactions with specific EGF-like repeats. Exp. Cell Res. 2005; 303:343–359. [PubMed: 15652348]

24. Cybulsky MI, et al. A major role for VCAM-1, but not ICAM-1, in early atherosclerosis. J. Clin. Invest. 2001; 107:1255–1262. [PubMed: 11375415]
25. Harris TA, Yamakuchi M, Ferlito M, Mendell JT, Lowenstein CJ. MicroRNA-126 regulates endothelial expression of vascular cell adhesion molecule 1. Proc. Natl. Acad. Sci. USA. 2008; 105:1516–1521. [PubMed: 18227515]
26. Ni CW, et al. Discovery of novel mechanosensitive genes in vivo using mouse carotid artery endothelium exposed to disturbed flow. Blood. 2010; 116:e66–e73. [PubMed: 20551377]
27. Sul HS. Minireview: Pref-1: role in adipogenesis and mesenchymal cell fate. Mol. Endocrinol. 2009; 23:1717–1725. [PubMed: 19541743]
28. Mortensen SB, et al. Membrane-tethered delta-like 1 homolog (DLK1) restricts adipose tissue size by inhibiting preadipocyte proliferation. Diabetes. 2012; 61:2814–2822. [PubMed: 22891218]
29. Rodríguez P, et al. The non-canonical NOTCH ligand DLK1 exhibits a novel vascular role as a strong inhibitor of angiogenesis. Cardiovasc. Res. 2012; 93:232–241. [PubMed: 22068159]
30. Qin L, et al. Notch1-mediated signaling regulates proliferation of porcine satellite cells (PSCs). Cell. Signal. 2013; 25:561–569. [PubMed: 23160004]
31. Nielsen LB. Transfer of low density lipoprotein into the arterial wall and risk of atherosclerosis. Atherosclerosis. 1996; 123:1–15. [PubMed: 8782833]
32. Zeng L, et al. Sustained activation of XBP1 splicing leads to endothelial apoptosis and atherosclerosis development in response to disturbed flow. Proc. Natl. Acad. Sci. USA. 2009; 106:8326–8331. [PubMed: 19416856]
33. Civelek M, Manduchi E, Riley RJ, Stoeckert CJ Jr, Davies PF. Chronic endoplasmic reticulum stress activates unfolded protein response in arterial endothelium in regions of susceptibility to atherosclerosis. Circ. Res. 2009; 105:453–461. [PubMed: 19661457]
34. Colles SM, Maxson JM, Carlson SG, Chisolm GM. Oxidized LDL-induced injury and apoptosis in atherosclerosis. Potential roles for oxysterols. Trends Cardiovasc. Med. 2001; 11:131–138.
35. Wei Y, et al. The microRNA-342-5p fosters inflammatory macrophage activation through an Akt1- and microRNA-155-dependent pathway during atherosclerosis. Circulation. 2013; 127:1609–1619. [PubMed: 23513069]
36. Jansen F, et al. Endothelial microparticle-mediated transfer of microRNA-126 promotes vascular endothelial cell repair via SPRED1 and is abrogated in glucose-damaged endothelial microparticles. Circulation. 2013; 128:2026–2038. [PubMed: 24014835]
37. Zhou J, et al. Regulation of vascular smooth muscle cell turnover by endothelial cell-secreted microRNA-126: role of shear stress. Circ. Res. 2013; 113:40–51. [PubMed: 23603512]
38. Fichtlscherer S, et al. Circulating microRNAs in patients with coronary artery disease. Circ. Res. 2010; 107:677–684. [PubMed: 20595655]
39. Zampetaki A, et al. Plasma microRNA profiling reveals loss of endothelial miR-126 and other microRNAs in type 2 diabetes. Circ. Res. 2010; 107:810–817. [PubMed: 20651284]
40. Mocharla P, et al. AngiomiR-126 expression and secretion from circulating $CD34^+$ and $CD14^+$ PBMCs: role for proangiogenic effects and alterations in type 2 diabetics. Blood. 2013; 121:226–236. [PubMed: 23144172]
41. Akhtar S, Gremse F, Kiessling F, Weber C, Schober A. CXCL12 promotes the stabilization of atherosclerotic lesions mediated by smooth muscle progenitor cells in Apoe-deficient mice. Arterioscler. Thromb. Vasc. Biol. 2013; 33:679–686. [PubMed: 23393393]
42. Schober A, Knarren S, Lietz M, Lin EA, Weber C. Crucial role of stroma cell-derived factor-1α in neointima formation after vascular injury in apolipoprotein E-deficient mice. Circulation. 2003; 108:2491–2497. [PubMed: 14581398]
43. Appelbe OK, Yevtodiyenko A, Muniz-Talavera H, Schmidt JV. Conditiona deletions refine the embryonic requirement for Dlk1. Mech. Dev. 2013; 130:143–159. [PubMed: 23059197]
44. Ehling M, Adams S, Benedito R, Adams RH. Notch controls retinal blood vessel maturation and quiescence. Development. 2013; 140:3051–3061. [PubMed: 23785053]
45. Nazari-Jahantigh M, et al. MicroRNA-155 promotes atherosclerosis by repressing Bcl6 in macrophages. J. Clin. Invest. 2012; 122:4190–4202. [PubMed: 23041630]

46. Nuovo G, Lee EJ, Lawler S, Godlewski J, Schmittgen T. *In situ* detection of mature microRNAs by labeled extension on ultramer templates. Biotechniques. 2009; 46:115–126. [PubMed: 19317656]

47. Gremse F, et al. Virtual elastic sphere processing enables reproducible quantification of vessel stenosis at CT and MR angiography. Radiology. 2011; 260:709–717. [PubMed: 21788527]

48. Schmitt MM, et al. Endothelial junctional adhesion molecule-a guides monocytes into flow-dependent predilection sites of atherosclerosis. Circulation. 2014; 129:66–76. [PubMed: 24065611]

49. Bidzhekov K, et al. Rafs constitute a nodal point in the regulation of embryonic endothelial progenitor cell growth and differentiation. J. Cell. Mol. Med. 2007; 11:1395–1407. [PubMed: 18205709]

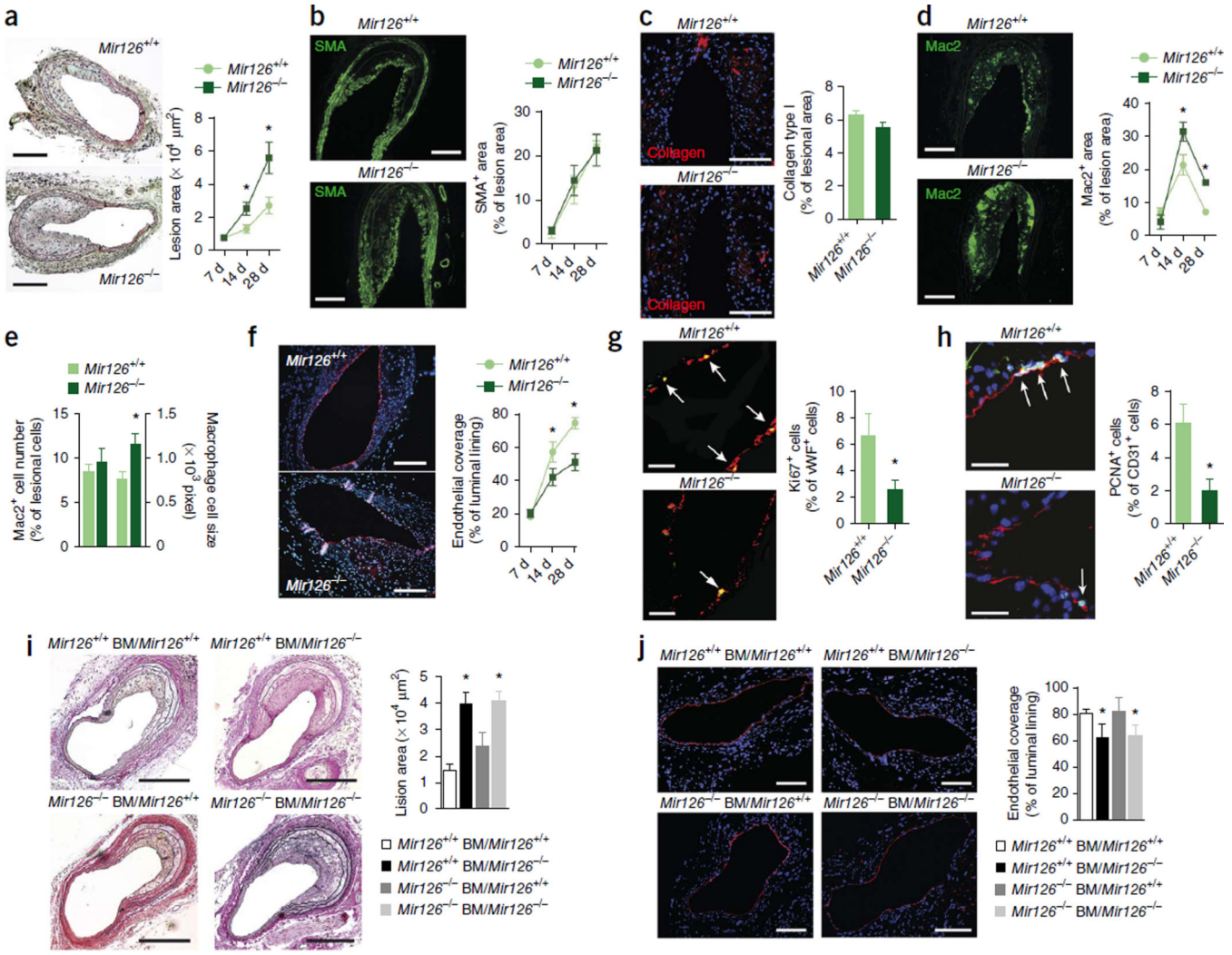

Figure 1.

Loss of endothelial miR-126 impairs endothelial repair in injured arteries. (**a–h**) Vascular repair after endothelial denudation of carotid arteries in *Mir126*$^{+/+}$ *Apoe*$^{-/-}$ (*Mir126*$^{+/+}$) and *Mir126*$^{-/-}$ *Apoe*$^{-/-}$ (*Mir126*$^{-/-}$) HCD-fed mice. (**a**) Lesion formation assessed by Movat's pentachrome staining (n = 6–7). (**b–d**) Lesional accumulation of SMCs (**b**; n = 3–7), collagen (**c**; n = 8) and Mac2+ macrophages (**d**; n = 3–6) determined by immunostaining. SMA, smooth muscle actin. (**e**) The number and size of lesional Mac2+ macrophages 28 d after injury (n = 4–6). (**f**) Endothelial repair after carotid injury assessed by mmunostaining for von Willebrand factor (vWF, red) (n = 6–7). (**g,h**) EC proliferation in carotid sections 28 d after injury assessed by double immunostaining for vWF (red) and Ki67 (green) (**g**; n = 6–7) or CD31 (red) and PCNA (green) (**h**; n = 8). Arrows indicate vWF+Ki67+ (**g**) and CD31+PCNA+ (**h**) cells. (**i,j**) Lesion areas (**i**) and endothelial coverage (**j**) in *Mir126*$^{+/+}$ and *Mir126*$^{-/-}$ mice reconstituted with *Mir126*$^{+/+}$ or *Mir126*$^{-/-}$ BM cells (*Mir126*$^{+/+}$ BM and *Mir126*$^{-/-}$BM, respectively) quantified 28 d after carotid injury by elastic van Gieson staining and CD31 immunostaining, respectively (n = 3–6 per group). Nuclei were stained with DAPI (blue). Ctrl, control. The data in **a–j** are represented as the mean ±s.e.m. of the

indicated number (*n*) of repeats. **P* < 0.05 by Student's *t* test (**a,d–h**) or one-way analysis of variance (ANOVA) (**i,j**). Scale bars, 10 μm (**g**); 20 μm (**h**); 100 μm (**a,c,j**); 200 μm (**b,d,f,i**).

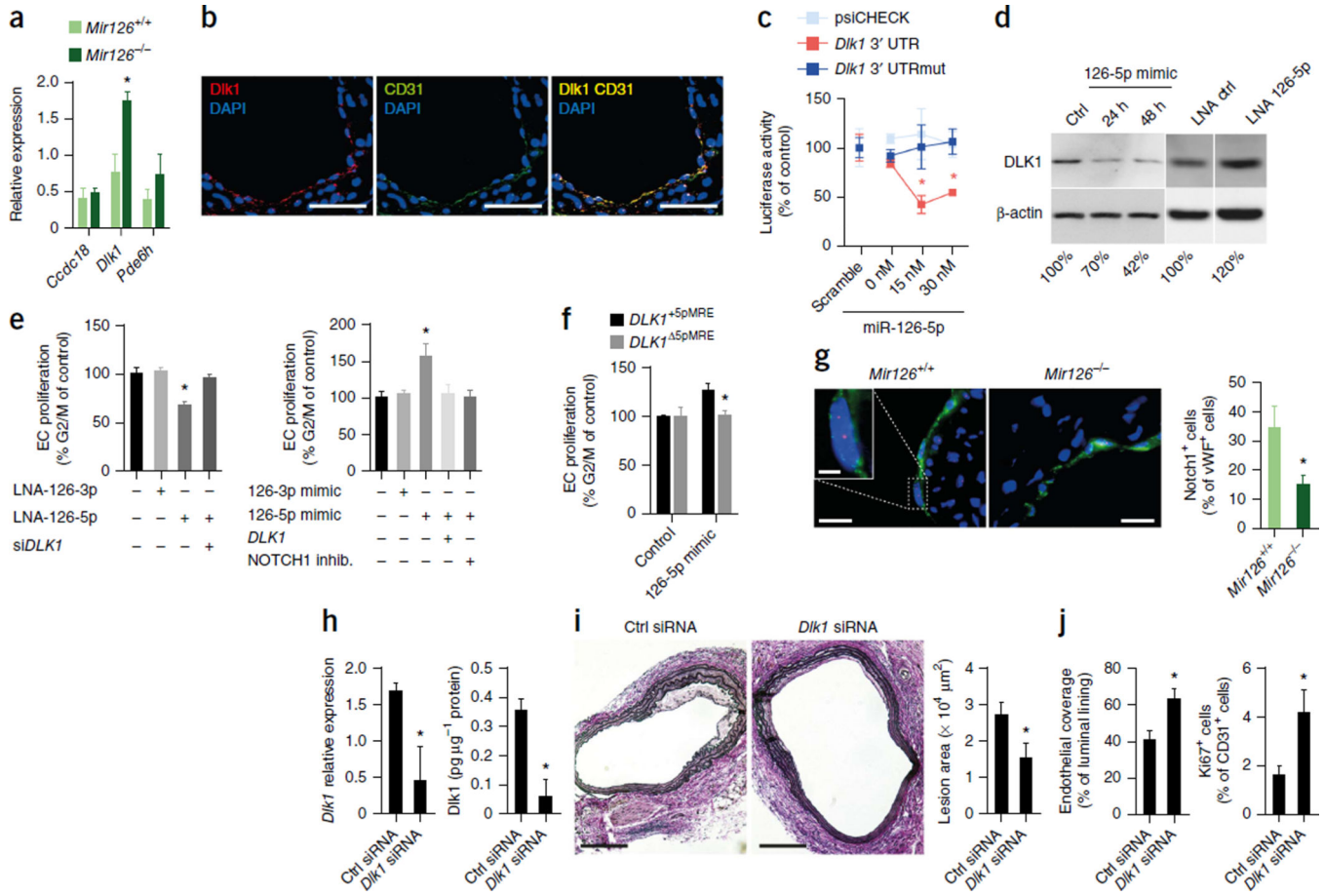

Figure 2.

The miR-126-5p target *Dlk1* inhibits endothelial repair. (**a,b**) Expression levels of *Ccdc18*, *Dlk1* and *Pde6h* mRNA (**a** $n = 4$) and immunostaining of Dlk1 and CD31 (**b**) in carotid arteries 14 d after injury. (**c**) The effect of miR-126-5p or a nonspecific control oligonucleotide (scramble) on luciferase activity in psiCHECK-transfected HEK293 cells expressing the wild-type or mutated 3′ UTR (UTRmut) of *Dlk1* ($n = 3$). (**d**) Immunoblot analysis of DLK1 and β-actin expression levels in HUVECs treated with a mimic or locked nucleic acid (LNA) inhibitor of miR-126-5p or a nonspecific control oligonucleotide (Ctrl). The numbers indicate DLK1 band intensities normalized to those of β-actin. (**e**) Flow cytometry analyses of EC proliferation after treatment of HUVECs with LNA inhibitors of miR-126-3p or miR-126-5p (LNA-126-3p and LNA-126-5p, respectively) with or without a *DLK1* -specific siRNA (si*DLK1*; $n = 3–7$) (left) or with miR-126-3p or miR-126-5p mimics with or without overexpression of *DLK1* or inhibition (inhib.) of NOTCH 1 ($n = 4–6$) (right). (**f**) Flow cytometry analysis of EC proliferation after treatment of HUVECs, which express *DLK1* with ($DLK1^{+5pMRE}$) or without ($DLK1^{\Delta 5pMRE}$) the miR-126-5p recognition element, with a control oligonucleotide or a miR-126-5p mimic ($n = 2–5$). (**g**) Double immunostaining of cleaved Notch1 (red) and vWF (green) in carotid arteries 14 d after injury ($n = 3–4$). (**h–j**) *Dlk1* mRNA expression (**h**; $n = 3–4$), Dlk1 protein expression (**h**; $n = 3$), lesion area (**i**; $n = 4–5$), endothelial recovery (CD31 immunostaining) (**i**; $n = 4–5$) and endothelial proliferation (**j**; $n = 4$) 14 d after injury of carotid arteries of *Mir126−/− Apoe*$^{-/-}$

mice treated with a nonspecific or *Dlk1*-specific siRNA. The data in **a, c** and **e–j** are represented as the mean ±s.e.m. of the indicated number (*n*) of repeats. **P* < 0.05 by Student's t test (**a,f–j**) or one-way ANOVA (**c,e**). Scale bars, 100 μm (**i**); 50 μm (**b**); 20 μm (g); 5 μm (**g**, inset).

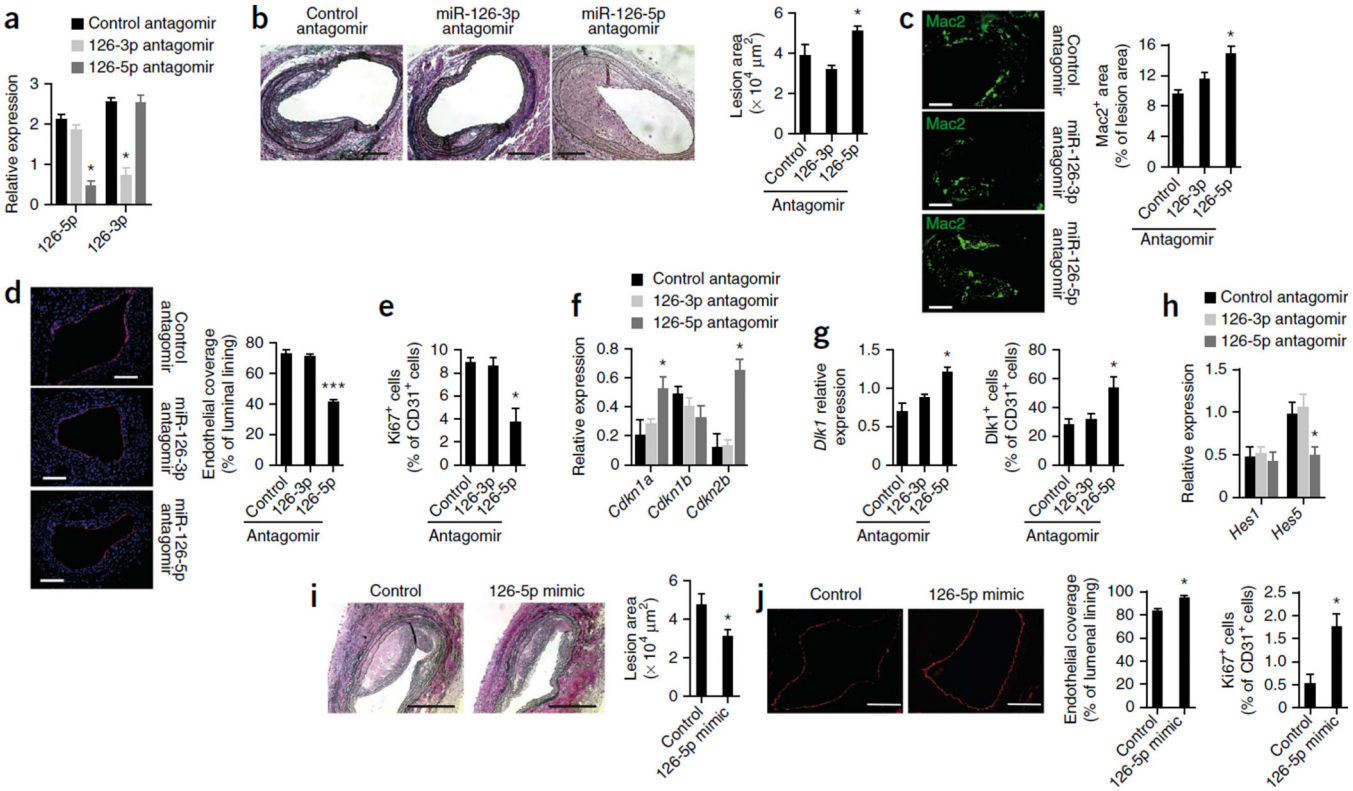

Figure 3.

The passenger strand miR-126-5p promotes endothelial repair. (**a–h**) The effects of local treatment of denuded arteries (28 d after carotid injury) from HCD-fed Apoe$^{-/-}$ mice with a nonspecific (control), miR-126-3p–specific or miR-126-5p–specific antagomir on miR-126-5pmiR-126-3p expression (**a**; n = 5–8), lesion formation (**b**; n = 4–6), lesional Mac2+ macrophage area (**c**; n = 3–7), endothelial coverage (CD31, red; DAPI, blue) (**d**; n = 4–6), endothelial proliferation (double staining for Ki67 and CD31) (**e**; n = 5–6), *Cdkn1a, Cdkn1b and Cdkn2b* mRNA expression (**f**; n = 3–4), *Dlk1* mRNA expression (**g**, left; n = 4), Dlk1 protein expression in ECs (double staining for Dlk1 and CD31) (**g**, right; n = 5–6) and *Hes1* and *Hes5* mRNA expression (**h**; n = 5–8). (**i,j**) Injured carotid arteries from HCD-fed *Apoe*$^{-/-}$ mice were treated perivascularly with a miR-126-5p mimic or control oligonucleotide for 28 d. (**i**) Lesion formation assessed by elastic van Gieson staining (n = 4). (**j**) Luminal endothelia coverage and endothelial proliferation rate determined by Ki67 and CD31 immunostaining (n = 4). All data are represented as the mean ± s.e.m. of the ndicated number (n) of repeats. *P < 0.05, ***P < 0.001 by one-way ANOVA (**a–h**) or Student's t test (**i,j**). Scale bars, 100 µm (**c,d,j**); 200 µm (**b,i**).

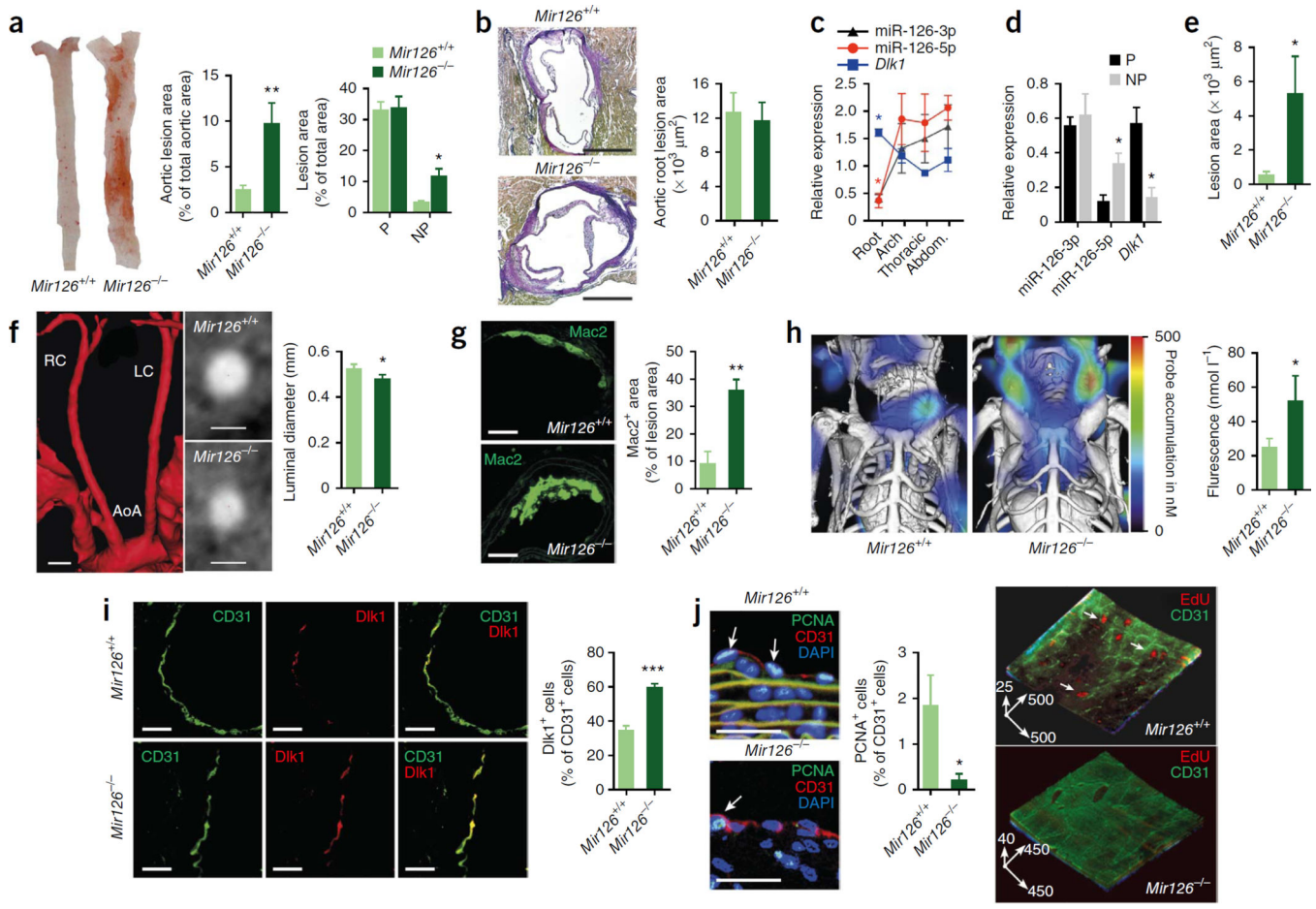

Figure 4.

Mir126 deficiency exacerbates atherosclerosis at nonpredilection sites. (**a–j**) Atherosclerotic lesions analyzed in *Mir126*$^{-/-}$ *Apoe*$^{-/-}$ and *Mir126*$^{+/+}$ *Apoe*$^{-/-}$ mice fed the HCD for 12 weeks. (**a,b**) Lesion formation at predilection (P) and nonpredilection (NP) sites in *en face* prepared aortas (**a**; n = 12–16) and aortic root sections (**b**; n = 11–12). (**c,d**) miR-126-5p, miR-126-3p and *Dlk1* expression in aortic regions (**c**; n = 3–4) and at P and NP sites (**d**; n = 3–5). Arch, aortic arch; abdom., abdominal aorta. (**e,f**) Lesion formation (**e**; n = 24–34) and luminal diameter (**f**; n = 18–30) of carotid arteries. Also shown are a three-dimensional reconstruction of the angiography (in red) of a *Mir126*$^{+/+}$ *Apoe*$^{-/-}$ mouse and images of cross-sections of the carotid arteries of *Mir126*$^{+/+}$ *Apoe*$^{-/-}$ and *Mir126*$^{-/-}$ *Apoe*$^{-/-}$ mice obtained by micro-computed tomography (**f**). AoA, aortic arch; LC, left carotid artery; RC, right carotid artery. (**g,h**) Lesional Mac2+ macrophage area (**g**; n = 4–5) and cathepsin activity in carotid arteries (**h**; n = 8–14). (**i,j**) Endothelial Dlk1 expression (**i**; n = 4) and endothelial proliferation in carotid arteries determined by immunostaining (**j**, left; n = 9–10) and by two-photon laser scanning microscopy (**j**, right; n = 4). The arrows in j indicate PCNA+ or 5-ethynyl-2'-deoxyuridine (EdU)+ ECs (**j**, left) or represent scale bars of a three-dimensional reconstruction (**j**, right; in µm). All data are represented as the mean ± s.e.m. of the indicated number (n) of repeats. *P < 0.05, **P < 0.01, ***P < 0.001 by Student's t test (**a,b,d–j**) or one-way ANOVA (**c**). Scale bars, 25 µm (**i,j**); 50 µm (**g**); 250 µm (**b**); 1 mm (**f**).

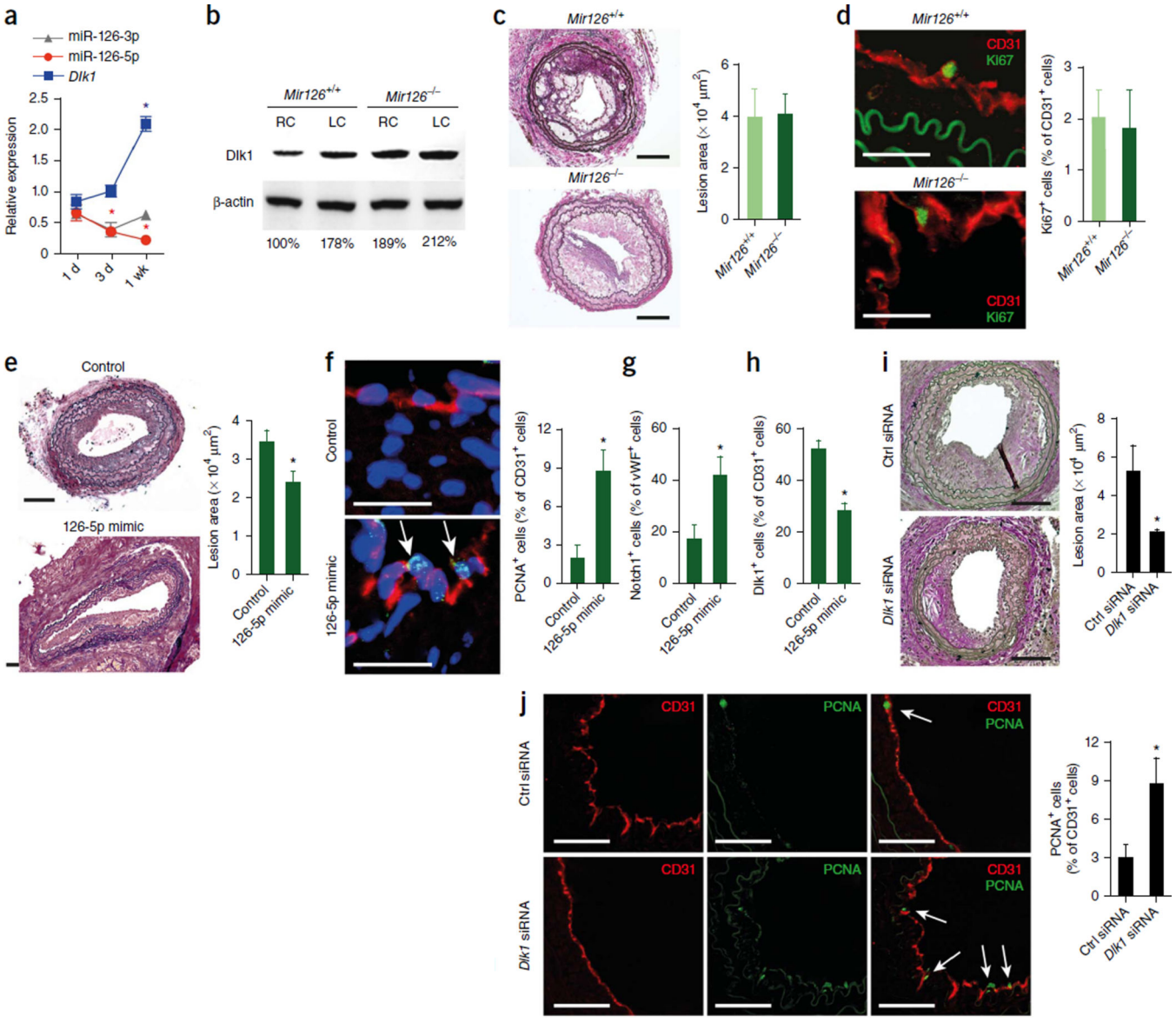

Figure 5.

Disturbed flow promotes atherosclerosis by downregulating miR-126-5p. (**a**) miR-126-5p, miR-126-3p and *Dlk1* expression in the carotid arteries of *Apoe*$^{-/-}$ mice after nducing disturbed flow by partial carotid ligation (n = 3–4). (**b**) Dlk1 protein expression 6 weeks after partial ligation of the left carotid artery (n = 3). Right carotid arteries were used as controls. The numbers indicate Dlk1 band intensities normalized to those of β-actin. (**c,d**) Lesion formation (**c**) and endothelia proliferation (**d**) after partial carotid ligation in *Mir126*$^{+/+}$ *Apoe*$^{-/-}$ and *Mir126*$^{-/-}$ *Apoe*$^{-/-}$ mice fed the HCD for 6 weeks (n = 4–6). (**e–h**) Lesion size (**e**), endothelial proliferation (**f**), Notch1 activation (**g**) and Dlk1 expression (**h**) in partially ligated carotid arteries of HCD-fed *Mir126*$^{-/-}$ *Apoe*$^{-/-}$ mice treated with a miR-126-5p mimic or a control oligonucleotide for 4 weeks (n = 3–4). (**i,j**) Lesion size (**i**) and EC proliferation (**j**) after partia igation of the carotid arteries of *Mir126*$^{+/+}$ *Apoe*$^{-/-}$ mice and treatment with a *Dlk1*-specific or nonspecific (Ctrl) siRNA (n = 5). Arrows in **f** and **j**

indicate $PCNA^{+}CD31^{+}$ cells. The data in **a** and **c–j** are represented as the mean ± s.e.m. of the indicated number (*n*) of repeats. **P* < 0.05 by one-way ANOVA (**a**) or Student's *t* test (**c–j**). Scale bars, 25 μm (**d,f**); 50 μm (**j**); 100 μm (**c,e,i**).

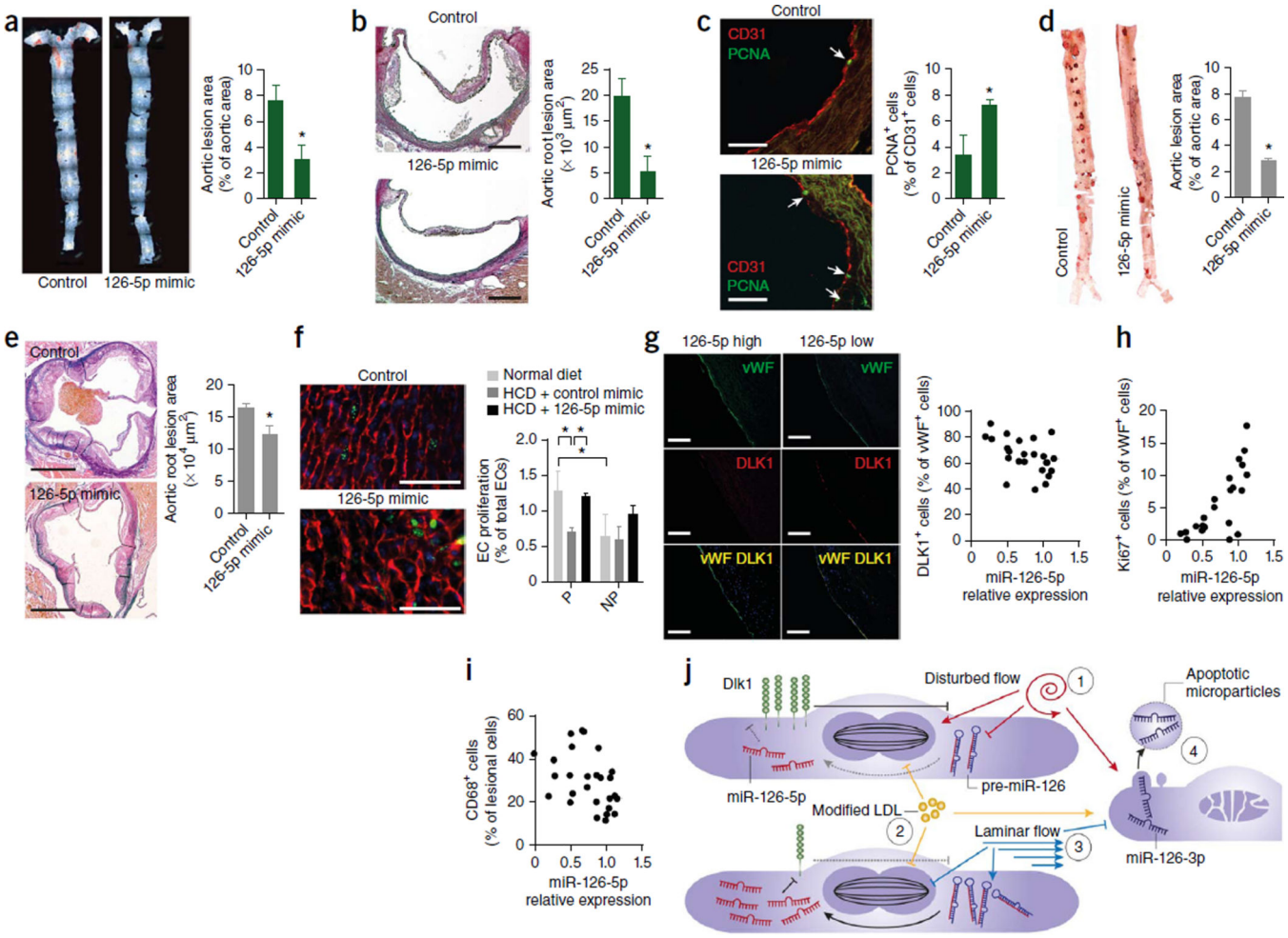

Figure 6.

Administration of miR-126-5p rescues EC proliferation during hyperlipidemic stress. (**a–c**) Lesion formation in *en face* prepared aortas (**a**) and aortic roots (**b**) and EC proliferation in aortic root sections (**c**) of HCD-fed *Mir126*$^{-/-}$ *Apoe*$^{-/-}$ mice systemically treated with a miR-126-5p mimic or a control oligonucleotide for 4 weeks (*n* = 3–4). The arrows in **c** indicate PCNA^{+} ECs. (**d,e**) Lesion formation in the thoracoabdominal aortas (**d**) and aortic roots (**e**) of *Mir126*$^{+/+}$ *Apoe*$^{-/-}$ mice treated with a miR-126-5p mimic or a control oligonucleotide for the last 4 weeks of a 12-week HCD feeding program (*n* = 3–4). (**f**) EC proliferation, detected by EdU (green) and CD31 (red) staining, at predilection and nonpredilection sites in *en face* prepared aortic arches of *Mir126*$^{+/+}$ *Apoe*$^{-/-}$ mice fed the HCD and treated with miR-126-5p mimics or control oligonucleotides and *Mir126*$^{+/+}$ *Apoe*$^{-/-}$ mice fed a normal diet (*n* = 3–4). (**g–i**) Correlation of the relative expression levels of miR-126-5p in human carotid lesions with endothelial DLK1 abundance (**g**; *n* = 24), EC proliferation (**h**; *n* = 22) and the percentage of lesional macrophages (**i**; *n* = 27). (**j**) Two-hit model of mpaired endothelial regeneration during atherosclerosis. Suppression of miR-126-5p in ECs at P sites counter-regulates the proliferative response to disturbed flow–induced injury by upregulating Dlk1 (1). This regenerative homeostasis is deranged by additional endothelial damage through hyperlipidemia (2). By contrast, laminar flow–

induced miR-126-5p at NP sites generates a proliferative reserve that maintains EC proliferation after hyperlipidemic stress (3). Increased apoptosis of ECs under disturbed flow but not under laminar flow conditions may result in the delivery of miR-126-3p by microparticles shed from apoptotic ECs, which may partially rescue the reduced endothelial regeneration at P sites (4). Endothelia cell proliferation is depicted by a representation of the mitotic spindle. Dashed and solid lines with bars indicate weak and strong inhibition, respectively. Arrows indicate activation. (**f,g**) Nuclei were stained with DAPI (blue). The data in **a–f** are represented as the mean ± s.e.m. of the ndicated number (*n*) of repeats. **P* < 0.05 by Student's *t* test. Scale bars, 50 μm (**c,f**); 200 μm (**b,g**); 500 μm (**e**).